HHS Public Access

Author manuscript

Brain Pathol. Author manuscript; available in PMC 2020 May 01.

Published in final edited form as:

Brain Pathol. 2019 May ; 29(3): 437–450. doi:10.1111/bpa.12677.

CLARITY REVEALS A MORE PROTRACTED TEMPORAL COURSE OF AXON SWELLING AND DISCONNECTION THAN PREVIOUSLY DESCRIBED FOLLOWING TRAUMATIC BRAIN INJURY

Maura T. Weber[#1], **John D. Arena**[#1], **Rui Xiao**[2], **John A. Wolf**[1,3], and **Victoria E. Johnson, MBChB, Ph.D.**[1]

[1]Department of Neurosurgery, Penn Center for Brain Injury and Repair, Perelman School of Medicine, University of Pennsylvania, Philadelphia, PA 19104, USA.

[2]The Department of Biostatistics, Epidemiology and Informatics, University of Pennsylvania, Philadelphia, PA 19104, USA.

[3]Corporal Michael J. Crescenz VA Medical Center, Philadelphia, PA 19104, USA

[#] These authors contributed equally to this work.

Abstract

Diffuse axonal injury (DAI) is an important consequence of traumatic brain injury (TBI). At the moment of trauma, axons rarely disconnect, but undergo cytoskeletal disruption and transport interruption leading to protein accumulation within swellings. The amyloid precursor protein (APP) accumulates rapidly and the standard histological evaluation of axonal pathology relies upon its detection. APP+ swellings first appear as varicosities along intact axons, which can ultimately undergo secondary disconnection to leave a terminal “axon bulb” at the disconnected, proximal end. However, sites of disconnection are difficult to determine with certainty using standard, thin tissue-sections, thus limiting the comprehensive evaluation of axon degeneration.

The tissue-clearing technology, CLARITY, permits three-dimensional visualization of axons that would otherwise be out of plane in standard tissue sections. Here, we examined the morphology and connection status of APP+ swellings using CLARITY at 6h, 24h, 1-week and 1-month following the controlled cortical impact (CCI) model of TBI in mice.

Remarkably, many APP+ swellings that appeared as terminal bulbs when viewed in standard 8μm-thick regions of tissue, were instead revealed to be varicose swellings along intact axons when three-dimensions were fully-visible. Moreover, the percentage of these potentially-viable axon swellings differed with survival from injury and may represent the delayed-onset of distinct mechanisms of degeneration. Even at 1-month post-CCI, ~10% of apparently terminal bulbs were revealed as connected by CLARITY and are thus potentially salvageable. Intriguingly, the

To whom correspondence should be addressed: Victoria E. Johnson, MBChB, Ph.D., Department of Neurosurgery, Penn Center for Brain Injury and Repair, 173 Stemmler Hall, 3450 Hamilton Walk, University of Pennsylvania, Philadelphia, PA 19104, USA, vje@pennmedicine.upenn.edu, Phone: +1 215-746-1866.

Conflicts of Interest: No authors have any conflicts of interest.

diameter of swellings decreased with survival, including varicosities along intact axons, and may reflect reversal of, or reduced, axonal transport interruption in the chronic setting.

These data indicate that APP immunohistochemistry on standard-thickness tissue sections overestimates axon disconnection, particularly acutely post-injury. Evaluating cleared tissue demonstrates a surprisingly delayed process of axon disconnection and thus longer window of therapeutic opportunity than previously appreciated. Intriguingly, a subset of axon swellings may also be capable of recovery.

INTRODUCTION

Diffuse axonal injury (DAI) is a common and important consequence of traumatic brain injury (TBI) and is associated with substantial morbidity (1, 3, 4, 28, 36, 37, 74). The progression of axonal pathology after TBI was originally characterized following severe injury and was thought to persist no longer than a few months (1, 3, 4). However, evidence of axonal injury has now been observed across the spectrum of TBI severity, including mild TBI or concussion, and axon degeneration has been observed many months and even years after injury in both humans and experimental models (6, 14, 32, 35, 37).

While axons rarely disconnect at the instant of trauma, the axonal cytoskeleton can undergo immediate mechanical disruption, including primary breaking of axonal microtubules (84, 85). In addition, TBI can induce progressive loss of ionic homeostasis in injured axons, including a massive influx of calcium ions that can drive calpain-mediated cytoskeletal degeneration and metabolic crisis (10, 13, 33, 39, 44, 45, 55, 66, 67, 71, 81, 87, 88). Adding further complexity, downstream events following severe TBI, including brain swelling and ischemic change, can be further injurious to axons (22, 23, 29, 31, 35, 64). All of these events can induce interruption of axonal transport leading to accumulation of transported cargos including the amyloid precursor protein (APP) and other proteins, which in turn causes swelling of the injured axons (15, 53, 80). Indeed, identification of APP immunoreactive (APP+) swollen axonal profiles in white matter has become the “gold standard” histological method to identify axonal pathology after TBI (26, 36, 69).

Initially appearing as tortuous or periodic, APP+ axonal swellings appear along axons that have not yet disconnected at the site of injury and are often referred to as “axonal varicosities”. It is thought that as some swellings increase in size and/or there is substantial proteolysis of the cytoskeleton, the axolemma can pinch off causing disconnection (56, 59). The swelling at the site of disconnection is often described as a terminal “axonal bulb” (previously “retraction ball”), beyond which the distal axon undergoes Wallerian degeneration (1, 2, 52, 54, 55, 57, 60, 61, 76, 77, 83). However, since standard paraffin tissue sections are typically only 6–10 microns thick, it is unclear whether purported axonal bulbs are truly disconnected, or if the axon continues out of plane from the relatively two-dimensional view.

The advent of tissue clearing technologies including CLARITY (17) can circumvent this limitation by allowing three-dimensional visualization of axon trajectories across what would otherwise be many tissue sections in standard histological approaches. By creating a

hydrogel-tissue hybrid and then selectively removing lipids from tissue, CLARITY produces optical transparency of thick or even whole-brain samples that can be subjected to immunostaining (17). Here, we utilized CLARITY to permit a fully three-dimensional view of the progression of axonal pathology following TBI. Specifically, we examined the temporal changes in morphology of transport-interrupted axons following controlled cortical impact (CCI) in the mouse up to 1-month post injury. This model relies on dynamic deformation of the cortical surface where primarily compressive forces induce mechanical injury to axons. Notably, these forces also cause a surface contusion with associated regional brain swelling, ischemic injury and inflammatory processes that may further compromise axons and recapitulate multiple aspects of the complex pathology of severe TBI. After first identifying apparently terminal APP+ axonal bulbs on 8μm thick regions of tissue, the true morphology and connection status of swellings was then re-evaluated with all three-dimensions fully visible through thick slices of cleared tissue. Results indicate that standard histological approaches overestimate the true extent of disconnected axonal bulbs relative to varicosities at all time points examined. Moreover, TBI induced a complex and multiphasic temporal course of axon swelling and disconnection post-CCI that is not only surprisingly protracted, but may have critical implications for the timing of potential therapeutic interventions and indicates that some swollen axons may be capable of recovery.

METHODS

All animal experiments were conducted in accordance with protocols approved by the University of Pennsylvania Institutional Animal Care and Use Committee and in accordance with the NIH Guide for the Care and Use of Laboratory Animals. Mice were housed in a temperature and humidity controlled facility with a 12-hour light / 12-hour dark cycle. Animal health was ensured via an established health monitoring program at the institution. Housed with 3–4 littermates, mice had free access to food and water throughout the duration of the study.

Controlled Cortical Impact (CCI) Model of TBI

Twelve week old CD1 male mice (39.46g ± 2.38g) (Charles River Laboratories, Wilmington, MA) were subjected to the established CCI model of TBI within a controlled laboratory environment as described in detail previously (79). Briefly, following induction using inhaled 5% isoflurane, mice were placed in a stereotaxic frame and maintenance anesthesia achieved using 2% isoflurane delivered via nose cone. Preemptive analgesia (buprenorphine: 0.1mg/kg) was administered subcutaneously. Under aseptic conditions, a 5mm craniectomy was performed midway between lambda and bregma and immediately lateral to the sagittal suture on the right side. With the head securely fixed, a cortical impact was performed at a 45° angle directly onto the intact dura using a metal impactor with a beveled 3mm diameter tip. The impact was driven via the release of pressurized nitrogen to a depth of 1mm at a velocity of $5ms^{-1}$ (CCI device model AMS-201: AmScien Instruments, Richmond, VA). Following clinical assessment, the incision site was sutured followed by withdrawal of anesthesia and appropriate post-surgical monitoring. All injuries were performed between 9am-12pm. Mice were survived for 6 hours, 24 hours, 1 week and 1 month post-CCI and compared with sham animals that underwent identical procedures

absent the cortical impact. Animals were assigned to groups randomly and in advance. No animals were excluded. Based on existing data, particularly the small variability in the outcomes observed among the animals, the proposed number of animals was anticipated to provide adequate power (90) (49). All subsequent histological experiments, analyses and quantification were performed blind to the injury status of the animal.

Tissue Handling Procedures

At the study endpoint, ketamine / xylazine / acepromazine (75/15/2 mg/kg, i.p.) was administered and following adequate anesthesia, animals were transcardially perfused with an initial flush of chilled 1X phosphate buffered saline (PBS) followed immediately by appropriate handling procedures to permit either:

1. **Standard Histological Analysis using Formalin Fixed Paraffin Embedded (FFPE) Tissue (CCI: n=4 per survival group; Shams: n=3 with 24h survival; n=5 with 1 month survival).** Animals were transcardially perfused with chilled 10% neutral buffered formalin (NBF), the brains extracted and post-fixed for 24 hours at 4ºC. Brains were subsequently blocked in the coronal plane and processed to paraffin using standard techniques. 8μm thick sections were obtained at the midpoint of the impact site using a rotary microtome.

2. **CLARITY (CCI: n=4 per survival group; Shams: n=3 with 24 hours survival):** Passive tissue clearance was performed as originally described by Chung et al (17). Animals underwent transcardial perfusion with 20ml of chilled hydrogel monomer solution (4% Acrylamide / 0.05% Bis-Acrylamide (Bio-Rad Laboratories, Hercules, CA) / 0.25% VA-044 Initiator (Wako Chemicals USA, Richmond, VA) / 4% paraformaldehyde / 1X PBS). Brains were extracted and post-fixed for a further 72 hours in hydrogel solution at 4ºC. The sample, immersed in hydrogel solution, was placed within a chamber where air was removed by vacuum and replaced with nitrogen as described (17). Subsequent incubation in a water bath was performed at 37ºC for 3 hours until the hydrogel monomer solution had polymerized. Brains were dissected into 2mm thick blocks in the coronal plane before being immersed in 50ml of clearing solution (4% sodium dodecyl sulphate, 200mM boric acid in deionized water, p.H 8.5) and incubated at 37ºC in a water bath. The solution was replaced every 3 days until tissue samples appeared transparent (Fig 1a,b). Samples were then rinsed in 0.1% TritonX in 1X PBS (PBST) and subsequently stored at 4ºC in PBST with sodium azide.

Standard Histological Examinations of FFPE Tissue

To characterize and verify reproducibility of the injury model, standard FFPE tissue was examined following staining with both hematoxylin and eosin (H&E) and Luxol Fast Blue / Cresyl Violet (LFB/CV) as described previously (35). The presence of brain atrophy over time was determined by measuring the area of the ipsilateral (injured) hemisphere as a percentage of the contralateral (uninjured) hemisphere using whole brain coronal sections at the epicenter of the impact site. Measurements were performed using ImageScope software (Leica Biosystems, Wetzlar, Germany) using whole-section, 20X high-resolution digital

scans acquired using the Aperio ScanScope (Leica Biosystems, Wetzlar, Germany). Immunohistochemical labelling of FFPE tissue was also performed to confirm the presence of axonal pathology using standard techniques as previously described (35, 37). Briefly, following deparaffinization and rehydration, endogenous peroxidase activity tissue was quenched using 3% aqueous hydrogen peroxide (15 minutes). Antigen retrieval was performed in a microwave pressure cooker with immersion in Tris EDTA buffer. Subsequent blocking was performed for 30 minutes in 1% normal horse serum (Vector Labs, Burlingame, CA, USA) in Optimax buffer (BioGenex, San Ramon, CA, USA). An additional blocking step was performed using M.O.M blocking reagent (Vector Labs, Burlingame, CA, USA) for labelling using mouse monoclonal antibodies on mouse tissue. Incubation with the primary antibodies was performed at 4ºC for 20 hours. Specifically, to identify axonal pathology, sections were labeled with an antibody reactive for the N-terminal amino acids 66–81 of the amyloid precursor protein (APP) (Clone 22C11(37, 75): Millipore, Billerica, MA) at 1:95k if visualized via 3,3'-diaminobenzidine (DAB) or 1:1K for immunofluorescence studies, and confirmed with goat anti-full length APP (70) at 1:1K (DAB). To identify normal axons, anti-neurofilament-heavy (NF-H) (Aves Lab, Tigard, OR, USA) was applied at 1:500 (immunofluorescence). After rinsing, sections were incubated with the appropriate biotinylated secondary antibody for 30 minutes followed by avidin-biotin complex and visualization achieved using DAB (all reagents: Vector Labs, Burlingame, CA, USA). Alternatively, the corresponding Alexa Fluor (Invitrogen, Carlsbad, CA) fluorescent secondary antibody was applied at 1:500 in a 2% species-specific serum solution for 2 hours at room temperature. Sections were rinsed and either dehydrated / cleared in xylenes before coverslipping in cytoseal or alternatively coverslipped using an aqueous mounting medium (Dako, Carpinteria, CA). Positive control tissue for APP IHC included sections of contused mouse tissue with previously established axonal pathology. Omission of subsets of primary antibodies was performed in positive control material to control for non-specific binding.

Immunofluorescent Labeling of Mouse Brain Tissue following CLARITY

Following CLARITY procedures, tissue was incubated in mouse anti-APP (22C11) primary antibody (1:100; Millipore, Billerica, MA, USA) and chicken anti-NFH primary antibody (1:50; Aves Lab, Tigard, OR, USA) in PBST for 72 hours at 37°C. Samples were then rinsed in PBST for 3 days at room temperature on a rocker before subsequent incubation in Alexa Fluor 488 donkey anti-mouse secondary antibody and Alexa Fluor 568 goat anti-chicken secondary antibodies (1:100; Invitrogen, Carlsbad, CA), for 4 days at 37°C. Samples were again rinsed in PBST for 3 days as above and stored in PBST with sodium azide until imaging.

Confocal Imaging

CLARITY tissue was immersed in FocusClear (Cedarlane, Burlington, NC) prior to confocal imaging. Notably, consistent with what has been described previously, the process of passive clearance results in tissue expansion, specifically during lipid-removal. In contrast, tissue shrinkage can occur with immersion in Focus Clear. Thus, in order to permit appropriate comparisons between samples and groups, all tissue, including from controls,

was handled using standardized protocols. Critically, this included a standardized pre-incubation in FocusClear for 1 hour immediately prior to imaging.

To minimize sample movement, tissue was positioned within a 2mm deep PDMS rectangle glued to a No. 1 coverslip and submerged in FocusClear (Cederlane Labs, Burlington, NC). Tissue was visualized using a confocal Nikon Eclipse Ti microscope (Nikon, Tokyo, Japan). High resolution confocal imaging was performed immediately adjacent to the focal contusion in an area measuring 630μm x630μm (1024×1024 pixels) at 1μm z-step intervals through 100μm of the tissue. FFPE tissue was also imaged throughout the 8μm tissue depth using the confocal microscope as above.

Quantification of CLARITY Immunofluorescence Findings

First, we sought to determine whether disconnected or terminal axonal bulbs identified in standard 8μm thick tissue sections are indeed truly disconnected axon terminals when viewed with the addition of a third dimension in space.

To achieve this, the peri-contusional 3D CLARITY confocal images (630μm x630μm x100μm) at 6 hours, 24 hours, 1 week, and 1 month post-CCI (n=4 per group) were first split into individual z-steps of 1μm thickness using Volocity 6.3 software (PerkinElemer, Waltham, MA, USA). Next, sets of eight consecutive z-steps were compressed to form 8μm thick images (via the max projection function) to represent the thickness of tissue typically examined when using standard FFPE sections.

These 8μm thick regions of cleared tissue were then examined for the presence of axonal bulbs. Consistent with historical descriptions, axon bulbs were defined as swollen spherical or ovoid axonal profiles that are APP immunoreactive and appear disconnected. An axon was considered swollen if its maximal diameter was greater than 3μm (at least 50% greater than the maximal diameter of normal axons as determined by the measurement of normal axons identified with NF-H IHC (n=336 axons) in cleared tissue from 2 sham mice).

Note, to avoid assessing individual bulbs twice, a 14μm deep gap was omitted between each 8μm thick image where apparently terminal bulbs were first identified. Similarly, the first 14μm was omitted from the top and bottom of the sample to ensure complete visualization of all bulbs when viewed in 3D (Fig 1c). This 14μm distance was determined based on maximal observed bulb size across all time points. The percentage of swellings that appeared terminal in these 8μm thick “FFPE equivalent” images in cleared tissue were compared to actual APP stained 8μm thick FFPE sections to ensure they were representative (Fig 1d,e).

Next, all apparently disconnected axonal bulbs identified on 8μm-thick cleared tissue regions were subsequently re-examined in 3D, with the full thickness of tissue visualized in the Z-axis through a 100μm depth of the imaged 3D CLARITY samples. Bulbs re-assessed in 3D were then designated as either: 1) confirmed as a disconnected or terminal axonal bulb with one or no visible projections or 2) re-designated as a connected varicose axonal swelling, having two clearly visible projections along an intact portion of axon. The

maximal diameter of all swellings was also measured using the line measurement tool in Volocity software (PerkinElemer, Waltham, MA, USA).

Statistical Analyses

The area of ipsilateral cortex as a percentage of the area of contralateral cortex was compared between groups as a metric of brain atrophy using 2-way ANOVA with Bonferroni correction for multiple comparisons. In addition, both the percentage of apparent bulbs on 8μm analyses that were revealed to have retained connectivity on 3D analysis, thus representing periodic varicose swellings, and the average bulb diameter were compared between groups using the linear mixed-effects model. This model takes into account the fact that each mouse had multiple measures by including a subject-specific random effect. Finally, logistic regression was used to assess associations of bulb diameter with the presence of revealed connectivity. Odds ratio with 95% confidence interval (CI) is reported.

Image Processing for Video

All supplemental videos were generated using Nikon NIS Elements AR software, Version 4.4 (Nikon, Tokyo, Japan). Regions of interest were selected on ND2 image files using the 3D volumetric view function and the video generated using the NIS Movie Maker function. Depth encoding was achieved (Video S1) by selecting the depth encoded max intensity projection tool. All supplemental video files were saved as AVI image file formats (.avi) using MPEG compression and subsequently converted to .mov files using Free MP4 Converter, Version 6.5.11 Aiseesoft Studio (Hong Kong). Final QuickTime files were generated using H.264 encoding with a resolution of 1280*720, video bitrate of 2500 kbps, frame rate of 30 fps, and aspect ratio of 16:9.

RESULTS

Clinical and Neuropathological Characterization of CCI in Mice

Immediately following CCI, no apnea beyond 30 seconds or clinical evidence of seizure was observed in any animals. All mice were ambulatory within 5–10 minutes of isoflurane withdrawal and resumed normal eating / drinking / grooming behaviors within 1 hour.

Standard (FFPE) histological characterization of mice (n=4 per group) revealed neuropathologies consistent with historical descriptions of the model. Specifically, acutely at 6 and 24 hours following CCI, a focal hemorrhagic contusion could be observed of approximately 5mm in diameter on the right cortical surface. Both grossly and on H&E examination, contusions could be observed throughout the full cortical thickness (Fig 2b,c.). By 1 week to 1 month following CCI, on both gross and histological (H&E and LFB/CV) examination, significant and progressive cavitation of the lesion site could be observed (Fig 2d,e,h.). Consistent with previous descriptions, measurements of brain atrophy demonstrated a significant and progressive loss of tissue out to 1 month post-injury (Fig 2f) (34, 40). APP IHC revealed extensive axonal pathology with tortuous varicose profiles and extensive axonal bulbs at 6 hours to 1 week post-CCI in peri-contusional cortex, underlying corpus callosum, hippocampus, as well as more minimally in the ipsilateral thalamus (Fig 2i). By 1 month post injury, while comparatively minimal, APP positive axonal bulbs and varicosities

could still be observed in the lesion site, predominantly surrounding the cavity and minimally in the underlying thalamus (Fig 2j). APP immunoreactive axonal pathology was absent in sham animals.

3D CLARITY Reveals that Axons are More Connected Post-CCI than Previously Appreciated using Standard Histological Approaches

Consistent with FFPE tissue, at all time points post-injury within cleared tissue, APP accumulation could be observed in injured or degenerating axons. Within 8μm-thick (FFPE-equivalent) tissue regions, APP accumulated within tortuous varicosities along axons that nonetheless remained intact or connected. However, much more frequently, APP accumulation was also observed in terminal axonal bulbs where only a single proximal process could be observed feeding into a disconnected, swollen axon terminus. In some cases, swellings appeared isolated with no clear projections (Fig 3d, Video S1–2). Importantly, there was no difference in the percentage of all axonal swellings that appeared terminal between images of standard 8μm-thick FFPE and images of 8μm-thick regions within CLARITY samples (n=4 per group at 24h survival $p = 0.59$).

However, when the same apparently-disconnected axonal bulbs observed in 8μm-thick regions were re-evaluated with the inclusion of the full third dimension in space (up to 100μm deep using the entire CLARITY image stack), a more complete appreciation of both axonal morphology and true axonal connectivity was ascertained. Specifically, in many instances these apparent axonal bulbs were revealed to have two clear processes and thus actually represented periodic varicose swellings along the length of an intact and thus potentially viable axon (Fig 3b,c, Video S3).

This was notably observed at all time points post-CCI. Specifically, 18.38 ± 2.27% of apparently terminal axonal bulbs identified on 8μm thick regions at 6 hours post-injury were revealed as intact varicosities when viewed in 3D up to 100μm deep. Intriguingly, by 24 hours post-CCI this number significantly increased, with 28.91 ± 3.25% of presumed disconnected bulbs revealed to be varicosities ($p=0.0002$) (Fig 3a).

In contrast, by 1 week only 9.36 ± 1.92% of bulbs were revealed to be varicosities, a significant decrease from both 6 ($p=0.0007$) and 24 hours ($p<0.0001$). Remarkably, this number remained stable out to 1 month post-CCI at 10.13 ± 1.07% (again significantly decreased from 6 hours ($p=0.0015$) and 24 hours ($p<0.0001$), but not significantly different from the 1 week survival time point ($p>0.9999$)) (Fig 3a).

Axonal Swellings Decrease in Size with Increased Survival Post-CCI

The diameter of axonal swellings was also observed to progressively decrease with survival post-CCI. This result was true in both swellings that were confirmed to be true axonal bulbs and those that were revealed to be connected, varicose swellings (Fig 4). Specifically, of the disconnected axonal bulbs, the mean diameter of swellings was significantly greater at 6 hours post-CCI (7.85 ± 0.43μm) versus those at 1 week (5.73 ±0.68μm, $p<0.001$) and 1 month (5.11 ± 0.52μm, $p<0.001$). In addition, bulbs at 24 hours post-CCI (7.01 ± 1.05μm) were significantly larger in diameter than those at 1 week ($p=0.042$) and month ($p=0.001$),

although did not differ from the 6 hour time point (p=0.13). No differences in diameter were observed between 1 week and 1 month (p=0.15) (Fig 4a).

Interestingly, apparent bulbs that were revealed to be varicosities in 3D (i.e. still connected both to both the proximal and distal axon) also underwent a progressive decrease in their maximal diameter over time, suggesting possible recovery. Swellings at 6 hours post-CCI (8.46 ± 0.42μm) were greater in diameter than those at 1 week (5.24 ± 0.52μm, p<0.001) and 1 month (5.59 ± 1.00μm, p<0.001). In addition, swellings at 24 hours post-CCI (7.59 ± 0.86μm) were also significantly larger in diameter than those at 1 week (5.24 ± 0.52μm, p<0.001) and 1 month (5.59 ± 1.00μm, p=0.003), although did not differ from the 6 hour time point (p=0.059). No differences in mean diameter were observed between 1 week and 1 month (p=0.64) (Fig 4b).

Decreased Maximal Diameter of Axonal Swellings is Associated with Disconnection

While bulb diameter decreased over time regardless of whether swellings were disconnected terminal bulbs or periodic varicose swellings, further analysis using logistic regression revealed that the diameter of individual axonal swellings was predictive of whether swellings were disconnected axonal bulbs or periodic varicose swellings along intact axons.

Specifically, axonal varicosities that initially appeared as terminal axonal bulbs on 8μm-thick regions, were more likely to be of increased diameter versus those swellings that were confirmed as disconnected axonal bulbs at 6 hours (p=0.018; OR 1.12; 95% CI 1.02–1.23), 24 hours (p=0.011; OR 1.09; 95% CI 1.02–1.16) and 1 month (p=0.018; OR 1.12; 95% CI 1.02–1.23) post-injury. However, there was no significant difference at the 1 week time point (p=0.24; OR 0.93; 95% CI 0.83–1.05).

While disconnection was associated with decreased overall diameter as described, individual data per mouse indicates that swellings with the smallest diameters occur less frequently in varicosities along intact axons at all time-points. In contrast, while swellings that were terminal had a wider range of sizes, this included many of the smallest swellings that may represent the small bead-like fragmentation that occurs in Wallerian degeneration.

Interestingly, by 1 week and 1 month, the extent of large swellings appears to be decreased in connected axons relative to those that are disconnected, with swellings having a narrower range of diameters, clustered in the lower range (Fig 5a–d). While this may reflect a less severely injured population of axons, it may also reflect recovery of transport.

DISCUSSION

Using the novel tissue clearing technology, CLARITY, the nature of axonal pathology after TBI in mice was found to be morphologically diverse and followed a surprisingly protracted time course. This complex array of swollen axonal phenotypes and their differential evolution post-TBI suggests multiple distinct mechanisms of degeneration, and intriguingly, possible reduced axonal transport interruption or recovery over time in some injured axons. Importantly, axonal swellings were observed along potentially salvageable, intact axons even at 1 month post-TBI, indicating a surprisingly long window of therapeutic opportunity.

By visualizing axonal pathology across three dimensions in space, we demonstrate that the extent of axonal disconnection is greatly overestimated when examined using conventional histological approaches on thin tissue sections. Specifically, 3D analyses utilizing thick blocks of cleared tissue, reveal that up to ~30% of axonal swellings appear to maintain connectivity post-CCI that were previously undetected with standard methods. While APP has emerged as a sensitive and early marker of axonal pathology (25, 37, 69), it is unknown whether all APP positive axonal swellings ultimately progress toward terminal disconnection, or whether a subset of these swellings are capable of undergoing repair with restoration of normal transport and function. Thus, an accurate appreciation of axon disconnection is critical when assessing both the degree of injury, as well as quantifying and interpreting histopathological outcome from experimental intervention.

Interestingly, the misidentification of varicose swellings as terminally disconnected axonal bulbs was not static over time, but rather had a variable temporal evolution out to 1 month post-injury. Specifically, at 6 hours post-CCI, ~20% of the swollen axons that appeared as terminal bulbs on thin sections were instead revealed to be varicosities along intact axons when viewed in full 3D. Curiously, this number increased significantly to ~30% at 24 hours, before declining to ~10% at 1 week and 1 month following injury. These data suggest that CCI causes an early (within 6h) and severe form of axonal degeneration with rapid transport interruption and disconnection, possibly due to direct mechanical perturbation of axonal cytoskeletal structure. This rapid disconnection appears to be followed shortly thereafter by a more protracted onset of axonal swellings, which may represent an emerging population of less-damaged axons undergoing a slower rate of APP accumulation and disconnection. In contrast, the delayed appearance of these swellings may also occur due to the multiple downstream pathophysiological processes including intra-axonal ionic imbalance, progressive cytoskeletal degradation, metabolic failure, oxidative stress and lipid peroxidation as described extensively following both in vivo and in vitro models of TBI (11, 12, 18–20, 33, 36, 37, 43, 47, 48, 50, 55, 66, 67, 74, 80, 81, 84, 85, 87, 88).

Understanding the temporal course of axonal disconnection in relation to specific mechanisms of degeneration will be critical for the optimization of timed therapeutic intervention. Remarkably, these data indicate that even 1 month following injury, a proportion of axonal swellings were not terminally disconnected and thus potentially recoverable. Previous studies have shown that tissue loss resulting from experimental contusions produced by focal impact models in rodents, including the CCI model, gradually increases over time, resulting in a dramatic and progressive atrophy persistent for up to one year after TBI (7, 8, 40, 72). This may be of particular clinical importance given that ongoing progressive brain atrophy has also been observed radiologically following brain injury in humans (5, 21, 86). Moreover, APP immunoreactive axonal pathology was recently demonstrated in association with marked atrophy in the corpus callosum, even many years after severe TBI in humans (35).

In addition to exploring the temporal course of axonal swelling and disconnection, examinations of cleared tissue revealed that the size of swellings also decreased with survival, regardless of whether swellings were terminally disconnected or remained attached to the distal axon. This may simply reflect an overall reduction in axonal transport in

severely damaged tissue, where multiple points of interruption limit the volume of APP available to feed into downstream swellings. More comprehensive sampling or whole-brain analysis of tracts will be important to further explore the relationship between serial swellings. While it is also possible that downstream Wallerian degeneration can induce smaller swellings along the fragmenting distal axon, recent examination of Thy1-YFP-H mice subjected to an impact model of TBI describes an absence of APP accumulation in distal axonal swellings otherwise identified by yellow fluorescent protein (30).

It is particularly noteworthy that swellings along intact axons, even at 1 week and 1 month post-injury, are smaller than those observed acutely. Indeed, swellings along intact axons were notably clustered in the smaller size-range when compared to disconnected bulbs, which typically encompassed a wider range of diameters. While this observation may indicate a population of less severely transport-interrupted axons with reduced disconnection, it also supports the intriguing possibility that some swellings decrease in size over time via recovery mechanisms that reinstate transport. While recovery of individual axonal swellings has yet to be directly observed post-TBI, temporal examinations of an impact model of TBI in rats suggest both physiological and morphological recovery is possible, with variable recovery reported between myelinated and unmyelinated axonal subpopulations (62, 63).

Observations in this study regarding the trajectory of axonal swelling and disconnection are dependent on the pathological events specific to the CCI injury model. Given both the biomechanical and neuropathological features of CCI, findings can most reasonably be extrapolated to the axonal pathology observed in contused human brain tissue. Specifically, CCI relies upon controlled contact loading to the dural surface to cause dynamic deformation of brain tissue over the course of ~10–30 milliseconds to induce the primary pathology of focal hemorrhagic cortical contusion (34, 79). Consistent with multiple previous reports (34, 41), extensive peri-contusional APP+ axonal pathology was observed immediately below the impact site, as well as more minimal axon damage in the underlying hippocampus and thalamus. Much of the early axonal pathology likely occurs due to the primary compressive forces caused by impact and associated downstream cascades. Specifically, tissue within the peri-contusional region also displays neuronal death, regional brain swelling and edema, ischemic change, blood brain barrier disruption, as well as diverse glial and inflammatory responses (34, 40, 79) that together comprise a complex pathological milieu that may be further detrimental to axons. Indeed, it has long been described that APP + axonal pathology can occur independently as a result of prolonged ischemia or secondary to the vascular complications of raised intracranial pressure (22, 23, 29, 31, 35, 64). As such, vascular compromise within the contused and peri-contusional tissue may contribute independently to acute axon degeneration following CCI.

An important source of axonal pathology in human TBI is that caused by rotational forces due to rapid acceleration / deceleration of the head at the moment of injury (24, 36, 37, 46, 65, 73, 78). Due to its large mass, the human brain is inherently vulnerable to this type of injury that contributes significantly to acute clinical outcome (24). However, acceleration / deceleration forces are absent during the fixed-head CCI model, and the degree of scaling required to generate clinically-relevant rotational forces in the smaller and lissencephalic

mouse brain are not feasible (34). Seminal studies have identified that forces from rotational accelerations are critical for the direct mechanical perturbation of axons to cause diffuse traumatic axonal injury (24, 37, 38, 46, 73). While not possible to examine using rodent cortical impact models as described here, determining how clinically-relevant rotational forces influence the trajectory of axon disconnection will be important to explore using appropriate models with a larger brain mass (37).

Furthermore, recent examination of both animal models and post-mortem human tissue demonstrates that APP does not label all swollen axons. Historically, multiple proteins have been identified accumulating in axonal swellings including various neurofilament subtypes (9–11, 13, 16, 27, 51, 58, 66, 82, 89), an N-terminal fragment of the alpha-spectrin protein (SNTF) (13, 37, 45, 66, 67, 87) and ubiquitin (68). However, APP was selected as a robust and early marker for diagnostic purposes and remains the “gold-standard” approach (25, 36, 69). Both specific neurofilament subtypes and SNTF have been shown to label distinct populations of APP-negative axonal swellings (37, 42, 82). Similarly, YFP+ axons in transgenic mice also displayed swellings that were APP-negative (30, 90). Thus, while APP labelling has been shown to identify the greatest number of swellings relative to other markers (37), it nonetheless fails to detect the entire population of injured axons within the models and time points examined thus far. Further elucidating whether these APP-negative axonal swellings have a different time course of degeneration and disconnection may permit a more comprehensive and informed approach to the neuropathological assessment of axonal pathology.

Here, we have demonstrated that 3D temporal examinations of post-traumatic axonal swelling and disconnection reveals novel insights into the timing and morphologies of axon degeneration beyond what can be observed with traditional histological approaches. Indeed, this approach provides unique opportunities for the further exploration of specific mechanisms and whole-brain effects of axonal injury. Understanding the temporal progression of axonal swelling may inform not only the optimal timing of early interventions, but suggests that future therapies may have utility beyond the acute-phase of injury.

Supplementary Material

Refer to Web version on PubMed Central for supplementary material.

ACKNOWLEDGEMENTS:

Research reported in this publication was supported by the National Institute of Neurological Disorders and Stroke of the National Institutes of Health under award number R01NS092398, R01NS094003, R01NS03810 and R01NS101108. In addition, work was supported in part by Merit Review, Award No. RX002705 (JAW) from the United States (U.S.) Department of Veterans Affairs, Rehabilitation Research and Development Service Program. The content is solely the responsibility of the authors and does not necessarily represent the official views of the National Institutes of Health, the U.S. Department of Veterans Affairs or the United States Government.

REFERENCES

1. Adams JH, Doyle D, Ford I, Gennarelli TA, Graham DI, McLellan DR (1989) Diffuse axonal injury in head injury: definition, diagnosis and grading. Histopathology15(1):49–59. [PubMed: 2767623]

2. Adams JH, Doyle D, Graham DI, al. e (1984) Diffuse axonal injury in head injuries caused by a fall. Lancet2:1420–2. [PubMed: 6151042]

3. Adams JH, Graham DI, Gennarelli TA, Maxwell WL (1991) Diffuse axonal injury in non-missile head injury. J Neurol Neurosurg Psychiatry54(6):481–3. [PubMed: 1880506]

4. Adams JH, Graham DI, Murray LS, Scott G (1982) Diffuse axonal injury due to nonmissile head injury in humans: an analysis of 45 cases. Ann Neurol12(6):557–63. [PubMed: 7159059]

5. Anderson CV, Bigler ED (1995) Ventricular dilation, cortical atrophy, and neuropsychological outcome following traumatic brain injury. J Neuropsychiatry Clin Neurosci7(1):42–8. [PubMed: 7711490]

6. Blumbergs PC, Scott G, Manavis J, Wainwright H, Simpson DA, McLean AJ (1994) Staining of amyloid precursor protein to study axonal damage in mild head injury. Lancet344(8929):1055–6. [PubMed: 7523810]

7. Bramlett HM, Dietrich WD (2002) Quantitative structural changes in white and gray matter 1 year following traumatic brain injury in rats. Acta neuropathologica103(6):607–14. [PubMed: 12012093]

8. Bramlett HM, Dietrich WD, Green EJ, Busto R (1997) Chronic histopathological consequences of fluid-percussion brain injury in rats: effects of post-traumatic hypothermia. Acta neuropathologica93(2):190–9. [PubMed: 9039468]

9. Buki A, Farkas O, Doczi T, Povlishock JT (2003) Preinjury administration of the calpain inhibitor MDL-28170 attenuates traumatically induced axonal injury. J Neurotrauma20(3):261–8. [PubMed: 12820680]

10. Buki A, Koizumi H, Povlishock JT (1999) Moderate posttraumatic hypothermia decreases early calpain-mediated proteolysis and concomitant cytoskeletal compromise in traumatic axonal injury. Exp Neurol159(1):319–28. [PubMed: 10486200]

11. Buki A, Okonkwo DO, Povlishock JT (1999) Postinjury cyclosporin A administration limits axonal damage and disconnection in traumatic brain injury. J Neurotrauma16(6):511–21. [PubMed: 10391367]

12. Buki A, Povlishock JT (2006) All roads lead to disconnection?--Traumatic axonal injury revisited. Acta neurochirurgica148(2):181–93; discussion 93–4. [PubMed: 16362181]

13. Buki A, Siman R, Trojanowski JQ, Povlishock JT (1999) The role of calpain-mediated spectrin proteolysis in traumatically induced axonal injury. Journal of neuropathology and experimental neurology58(4):365–75. [PubMed: 10218632]

14. Chen XH, Johnson VE, Uryu K, Trojanowski JQ, Smith DH (2009) A lack of amyloid beta plaques despite persistent accumulation of amyloid beta in axons of long-term survivors of traumatic brain injury. Brain Pathol19(2):214–23. [PubMed: 18492093]

15. Christman CW, Grady MS, Walker SA, Holloway KL, Povlishock JT (1994) Ultrastructural studies of diffuse axonal injury in humans. J Neurotrauma11(2):173–86. [PubMed: 7523685]

16. Christman CW, Salvant JB Jr., Walker SA, Povlishock JT (1997) Characterization of a prolonged regenerative attempt by diffusely injured axons following traumatic brain injury in adult cat: a light and electron microscopic immunocytochemical study. Acta neuropathologica94(4):329–37. [PubMed: 9341933]

17. Chung K, Wallace J, Kim SY, Kalyanasundaram S, Andalman AS, Davidson TJ, Mirzabekov JJ, Zalocusky KA, Mattis J, Denisin AK, Pak S, Bernstein H, Ramakrishnan C, Grosenick L, Gradinaru V, Deisseroth K (2013) Structural and molecular interrogation of intact biological systems. Nature497(7449):332–7. [PubMed: 23575631]

18. Deng-Bryant Y, Singh IN, Carrico KM, Hall ED (2008) Neuroprotective effects of tempol, a catalytic scavenger of peroxynitrite-derived free radicals, in a mouse traumatic brain injury model. J Cereb Blood Flow Metab28(6):1114–26. [PubMed: 18319733]

19. Deng Y, Thompson BM, Gao X, Hall ED (2007) Temporal relationship of peroxynitrite-induced oxidative damage, calpain-mediated cytoskeletal degradation and neurodegeneration after traumatic brain injury. Exp Neurol205(1):154–65. [PubMed: 17349624]

20. Fujita M, Oda Y, Wei EP, Povlishock JT The combination of either tempol or FK506 with delayed hypothermia: implications for traumatically induced microvascular and axonal protection. J Neurotrauma28(7):1209–18.

21. Gale SD, Johnson SC, Bigler ED, Blatter DD (1995) Nonspecific white matter degeneration following traumatic brain injury. J Int Neuropsychol Soc1(1):17–28. [PubMed: 9375205]
22. Geddes JF, Vowles GH, Beer TW, Ellison DW (1997) The diagnosis of diffuse axonal injury: implications for forensic practice. Neuropathology and applied neurobiology23(4):339–47. [PubMed: 9292874]
23. Geddes JF, Whitwell HL, Graham DI (2000) Traumatic axonal injury: practical issues for diagnosis in medicolegal cases. Neuropathol Appl Neurobiol26(2):105–16. [PubMed: 10840273]
24. Gennarelli TA, Thibault LE, Adams JH, Graham DI, Thompson CJ, Marcincin RP (1982) Diffuse axonal injury and traumatic coma in the primate. Ann Neurol12(6):564–74. [PubMed: 7159060]
25. Gentleman SM, Nash MJ, Sweeting CJ, Graham DI, Roberts GW (1993) Beta-amyloid precursor protein (beta APP) as a marker for axonal injury after head injury. Neurosci Lett160(2):139–44. [PubMed: 8247344]
26. Gentleman SM, Roberts GW, Gennarelli TA, Maxwell WL, Adams JH, Kerr S, Graham DI (1995) Axonal injury: a universal consequence of fatal closed head injury? Acta neuropathologica89(6): 537–43. [PubMed: 7676809]
27. Grady MS, McLaughlin MR, Christman CW, Valadka AB, Fligner CL, Povlishock JT (1993) The use of antibodies targeted against the neurofilament subunits for the detection of diffuse axonal injury in humans. Journal of neuropathology and experimental neurology52(2):143–52. [PubMed: 8440996]
28. Graham DI, Adams JH, Nicoll JA, Maxwell WL, Gennarelli TA (1995) The nature, distribution and causes of traumatic brain injury. Brain Pathol5(4):397–406. [PubMed: 8974622]
29. Graham DI, Smith C, Reichard R, Leclercq PD, Gentleman SM (2004) Trials and tribulations of using beta-amyloid precursor protein immunohistochemistry to evaluate traumatic brain injury in adults. Forensic Sci Int146(2–3):89–96. [PubMed: 15542268]
30. Greer JE, McGinn MJ, Povlishock JT (2011) Diffuse traumatic axonal injury in the mouse induces atrophy, c-Jun activation, and axonal outgrowth in the axotomized neuronal population. J Neurosci31(13):5089–105. [PubMed: 21451046]
31. Hayashi T, Ago K, Ago M, Ogata M (2009) Two patterns of beta-amyloid precursor protein (APP) immunoreactivity in cases of blunt head injury. Leg Med (Tokyo)11 Suppl 1:S171–3. [PubMed: 19251455]
32. Iwata A, Chen XH, McIntosh TK, Browne KD, Smith DH (2002) Long-term accumulation of amyloid-beta in axons following brain trauma without persistent upregulation of amyloid precursor protein genes. Journal of neuropathology and experimental neurology61(12):1056–68. [PubMed: 12484568]
33. Iwata A, Stys PK, Wolf JA, Chen XH, Taylor AG, Meaney DF, Smith DH (2004) Traumatic axonal injury induces proteolytic cleavage of the voltage-gated sodium channels modulated by tetrodotoxin and protease inhibitors. J Neurosci24(19):4605–13. [PubMed: 15140932]
34. Johnson VE, Meaney DF, Cullen DK, Smith DH (2015) Animal models of traumatic brain injury. Handbook of clinical neurology127:115–28. [PubMed: 25702213]
35. Johnson VE, Stewart JE, Begbie FD, Trojanowski JQ, Smith DH, Stewart W (2013) Inflammation and white matter degeneration persist for years after a single traumatic brain injury. Brain136(1): 28–42. [PubMed: 23365092]
36. Johnson VE, Stewart W, Smith DH (2013) Axonal pathology in traumatic brain injury. Exp Neurol246:35–43. [PubMed: 22285252]
37. Johnson VE, Stewart W, Weber MT, Cullen DK, Siman R, Smith DH (2016) SNTF immunostaining reveals previously undetected axonal pathology in traumatic brain injury. Acta neuropathologica131(1):115–35. [PubMed: 26589592]
38. Johnson VE, Weber MT, Xiao R, Cullen DK, Meaney DF, Stewart W, Smith DH (2018) Mechanical disruption of the blood-brain barrier following experimental concussion. Acta neuropathologica135(5):711–26. [PubMed: 29460006]
39. Kampfl A, Posmantur R, Nixon R, Grynspan F, Zhao X, Liu SJ, Newcomb JK, Clifton GL, Hayes RL (1996) mu-calpain activation and calpain-mediated cytoskeletal proteolysis following traumatic brain injury. J Neurochem67(4):1575–83. [PubMed: 8858942]

40. Loane DJ, Kumar A, Stoica BA, Cabatbat R, Faden AI (2014) Progressive neurodegeneration after experimental brain trauma: association with chronic microglial activation. Journal of neuropathology and experimental neurology73(1):14–29. [PubMed: 24335533]
41. Mac Donald CL, Dikranian K, Song SK, Bayly PV, Holtzman DM, Brody DL (2007) Detection of traumatic axonal injury with diffusion tensor imaging in a mouse model of traumatic brain injury. Exp Neurol205(1):116–31. [PubMed: 17368446]
42. Marmarou CR, Walker SA, Davis CL, Povlishock JT (2005) Quantitative analysis of the relationship between intra-axonal neurofilament compaction and impaired axonal transport following diffuse traumatic brain injury. J Neurotrauma22(10):1066–80. [PubMed: 16238484]
43. Maxwell WL, Domleo A, McColl G, Jafari SS, Graham DI (2003) Post-acute alterations in the axonal cytoskeleton after traumatic axonal injury. J Neurotrauma20(2):151–68. [PubMed: 12675969]
44. Maxwell WL, Watt C, Pediani JD, Graham DI, Adams JH, Gennarelli TA (1991) Localisation of calcium ions and calcium-ATPase activity within myelinated nerve fibres of the adult guinea-pig optic nerve. J Anat176:71–9. [PubMed: 1833365]
45. McGinn MJ, Kelley BJ, Akinyi L, Oli MW, Liu MC, Hayes RL, Wang KK, Povlishock JT (2009) Biochemical, structural, and biomarker evidence for calpain-mediated cytoskeletal change after diffuse brain injury uncomplicated by contusion. Journal of neuropathology and experimental neurology68(3):241–9. [PubMed: 19225412]
46. Meaney DF, Smith DH, Shreiber DI, Bain AC, Miller RT, Ross DT, Gennarelli TA (1995) Biomechanical analysis of experimental diffuse axonal injury. J Neurotrauma12(4):689–94. [PubMed: 8683620]
47. Mustafa AG, Singh IN, Wang J, Carrico KM, Hall ED Mitochondrial protection after traumatic brain injury by scavenging lipid peroxyl radicals. J Neurochem114(1):271–80. [PubMed: 20403083]
48. Mustafa AG, Wang JA, Carrico KM, Hall ED Pharmacological inhibition of lipid peroxidation attenuates calpain-mediated cytoskeletal degradation after traumatic brain injury. J Neurochem117(3):579–88. [PubMed: 21361959]
49. Nakagawa Y, Nakamura M, McIntosh TK, Rodriguez A, Berlin JA, Smith DH, Saatman KE, Raghupathi R, Clemens J, Saido TC, Schmidt ML, Lee VM, Trojanowski JQ (1999) Traumatic brain injury in young, amyloid-beta peptide overexpressing transgenic mice induces marked ipsilateral hippocampal atrophy and diminished Abeta deposition during aging. J Comp Neurol411(3):390–8. [PubMed: 10413774]
50. Okonkwo DO, Povlishock JT (1999) An intrathecal bolus of cyclosporin A before injury preserves mitochondrial integrity and attenuates axonal disruption in traumatic brain injury. J Cereb Blood Flow Metab19(4):443–51. [PubMed: 10197514]
51. Pettus EH, Christman CW, Giebel ML, Povlishock JT (1994) Traumatically induced altered membrane permeability: its relationship to traumatically induced reactive axonal change. J Neurotrauma11(5):507–22. [PubMed: 7861444]
52. Povlishock JT (1992) Traumatically induced axonal injury: pathogenesis and pathobiological implications. Brain Pathol2:1–12. [PubMed: 1341941]
53. Povlishock JT, Becker DP (1985) Fate of reactive axonal swellings induced by head injury. Lab Invest52(5):540–52. [PubMed: 2581065]
54. Povlishock JT, Becker DP, Cheng CLY, Vaughan GW (1983) Axonal change in minor head injury. JNeuropatholExpNeurol42:225–42.
55. Povlishock JT, Buki A, Koiziumi H, Stone J, Okonkwo DO (1999) Initiating mechanisms involved in the pathobiology of traumatically induced axonal injury and interventions targeted at blunting their progression. Acta Neurochir Suppl73:15–20. [PubMed: 10494336]
56. Povlishock JT, Christman CW (1995) The pathobiology of traumatically induced axonal injury in animals and humans: a review of current thoughts. J Neurotrauma12(4):555–64. [PubMed: 8683606]
57. Povlishock JT, Katz DI (2005) Update of neuropathology and neurological recovery after traumatic brain injury. J Head Trauma Rehabil20(1):76–94. [PubMed: 15668572]

58. Povlishock JT, Marmarou A, McIntosh T, Trojanowski JQ, Moroi J (1997) Impact acceleration injury in the rat: evidence for focal axolemmal change and related neurofilament sidearm alteration. Journal of neuropathology and experimental neurology56(4):347–59. [PubMed: 9100665]
59. Povlishock JT, Pettus EH (1996) Traumatically induced axonal damage: evidence for enduring changes in axolemmal permeability with associated cytoskeletal change. Acta Neurochir Suppl. 66:81–6. [PubMed: 8686530]
60. Ramon Y Cajal S (1928) Degeneration and regeneration in the nervous system, Oxford university press: Oxford, UK.
61. Rand CW, Courville CB (1946) Histologic changes in the brain in cases of fatal injury to the head; alterations in nerve cells. Arch Neurol Psychiatry55:79–110.
62. Reeves TM, Phillips LL, Povlishock JT (2005) Myelinated and unmyelinated axons of the corpus callosum differ in vulnerability and functional recovery following traumatic brain injury. Exp Neurol196(1):126–37. [PubMed: 16109409]
63. Reeves TM, Smith TL, Williamson JC, Phillips LL (2012) Unmyelinated axons show selective rostrocaudal pathology in the corpus callosum after traumatic brain injury. Journal of neuropathology and experimental neurology71(3):198–210. [PubMed: 22318124]
64. Reichard RR, Smith C, Graham DI (2005) The significance of beta-APP immunoreactivity in forensic practice. Neuropathology and applied neurobiology31(3):304–13. [PubMed: 15885067]
65. Ross DT, Meaney DF, Sabol MK, Smith DH, Gennarelli TA (1994) Distribution of forebrain diffuse axonal injury following inertial closed head injury in miniature swine. Exp Neurol126(2): 291–9. [PubMed: 7925827]
66. Saatman KE, Abai B, Grosvenor A, Vorwerk CK, Smith DH, Meaney DF (2003) Traumatic axonal injury results in biphasic calpain activation and retrograde transport impairment in mice. J Cereb Blood Flow Metab23(1):34–42. [PubMed: 12500089]
67. Saatman KE, Bozyczko-Coyne D, Marcy V, Siman R, McIntosh TK (1996) Prolonged calpain-mediated spectrin breakdown occurs regionally following experimental brain injury in the rat. Journal of neuropathology and experimental neurology55(7):850–60. [PubMed: 8965100]
68. Schweitzer JB, Park MR, Einhaus SL, Robertson JT (1993) Ubiquitin marks the reactive swellings of diffuse axonal injury. Acta neuropathologica85(5):503–7. [PubMed: 8388148]
69. Sherriff FE, Bridges LR, Sivaloganathan S (1994) Early detection of axonal injury after human head trauma using immunocytochemistry for beta-amyloid precursor protein. Acta Neuropathol (Berl)87(1):55–62. [PubMed: 8140894]
70. Shoji M, Golde TE, Ghiso J, Cheung TT, Estus S, Shaffer LM, Cai XD, McKay DM, Tintner R, Frangione B, et al. (1992) Production of the Alzheimer amyloid beta protein by normal proteolytic processing. Science258(5079):126–9. [PubMed: 1439760]
71. Singleton RH, Stone JR, Okonkwo DO, Pellicane AJ, Povlishock JT (2001) The immunophilin ligand FK506 attenuates axonal injury in an impact-acceleration model of traumatic brain injury. J Neurotrauma18(6):607–14. [PubMed: 11437083]
72. Smith DH, Chen XH, Pierce JE, Wolf JA, Trojanowski JQ, Graham DI, McIntosh TK (1997) Progressive atrophy and neuron death for one year following brain trauma in the rat. J Neurotrauma14(10):715–27. [PubMed: 9383090]
73. Smith DH, Chen XH, Xu BN, McIntosh TK, Gennarelli TA, Meaney DF (1997) Characterization of diffuse axonal pathology and selective hippocampal damage following inertial brain trauma in the pig. Journal of neuropathology and experimental neurology56(7):822–34. [PubMed: 9210879]
74. Smith DH, Hicks R, Povlishock JT (2013) Therapy development for diffuse axonal injury. J Neurotrauma30(5):307–23. [PubMed: 23252624]
75. Smith DH, Johnson VE, Stewart W (2013) Chronic neuropathologies of single and repetitive TBI: substrates of dementia? Nature Reviews Neurology9(4):211–21. [PubMed: 23458973]
76. Smith DH, Meaney DF (2000) Axonal damage in traumatic brain injury. The neuroscientist 6:483–95.
77. Smith DH, Meaney DF, Shull WH (2003) Diffuse axonal injury in head trauma. J Head Trauma Rehabil18(4):307–16. [PubMed: 16222127]

78. Smith DH, Nonaka M, Miller R, Leoni M, Chen XH, Alsop D, Meaney DF (2000) Immediate coma following inertial brain injury dependent on axonal damage in the brainstem. Journal of neurosurgery93(2):315–22. [PubMed: 10930019]

79. Smith DH, Soares HD, Pierce JS, Perlman KG, Saatman KE, Meaney DF, Dixon CE, McIntosh TK (1995) A model of parasagittal controlled cortical impact in the mouse: cognitive and histopathologic effects. J Neurotrauma12(2):169–78. [PubMed: 7629863]

80. Smith DH, Wolf JA, Lusardi TA, Lee VM, Meaney DF (1999) High tolerance and delayed elastic response of cultured axons to dynamic stretch injury. J Neurosci19(11):4263–9. [PubMed: 10341230]

81. Staal JA, Dickson TC, Gasperini R, Liu Y, Foa L, Vickers JC (2010) Initial calcium release from intracellular stores followed by calcium dysregulation is linked to secondary axotomy following transient axonal stretch injury. J Neurochem112(5):1147–55. [PubMed: 19968758]

82. Stone JR, Singleton RH, Povlishock JT (2001) Intra-axonal neurofilament compaction does not evoke local axonal swelling in all traumatically injured axons. Exp Neurol172(2):320–31. [PubMed: 11716556]

83. Strich SJ (1956) Diffuse degeneration of the cerebral white matter in severe dementia following head injury. J Neurol Neurosurg Psychiatry19(3):163–85. [PubMed: 13357957]

84. Tang-Schomer MD, Johnson VE, Baas PW, Stewart W, Smith DH (2012) Partial interruption of axonal transport due to microtubule breakage accounts for the formation of periodic varicosities after traumatic axonal injury. Exp Neurol233(1):364–72. [PubMed: 22079153]

85. Tang-Schomer MD, Patel AR, Baas PW, Smith DH (2010) Mechanical breaking of microtubules in axons during dynamic stretch injury underlies delayed elasticity, microtubule disassembly, and axon degeneration. FASEB J24(5):1401–10. [PubMed: 20019243]

86. Tomaiuolo F, Bivona U, Lerch JP, Di Paola M, Carlesimo GA, Ciurli P, Matteis M, Cecchetti L, Forcina A, Silvestro D, Azicnuda E, Sabatini U, Di Giacomo D, Caltagirone C, Petrides M, Formisano R (2012) Memory and anatomical change in severe non missile traumatic brain injury: approximately 1 vs. approximately 8 years follow-up. Brain Res Bull87(4–5):373–82. [PubMed: 22289841]

87. von Reyn CR, Spaethling JM, Mesfin MN, Ma M, Neumar RW, Smith DH, Siman R, Meaney DF (2009) Calpain mediates proteolysis of the voltage-gated sodium channel alpha-subunit. J Neurosci29(33):10350–6. [PubMed: 19692609]

88. Wolf JA, Stys PK, Lusardi T, Meaney D, Smith DH (2001) Traumatic axonal injury induces calcium influx modulated by tetrodotoxin-sensitive sodium channels. J Neurosci21(6):1923–30. [PubMed: 11245677]

89. Yaghmai A, Povlishock J (1992) Traumatically induced reactive change as visualized through the use of monoclonal antibodies targeted to neurofilament subunits. Journal of neuropathology and experimental neurology51(2):158–76. [PubMed: 1538240]

90. Ziogas NK, Koliatsos VE (2018) Primary Traumatic Axonopathy in Mice Subjected to Impact Acceleration: A Reappraisal of Pathology and Mechanisms with High-Resolution Anatomical Methods. J Neurosci38(16):4031–47. [PubMed: 29567804]

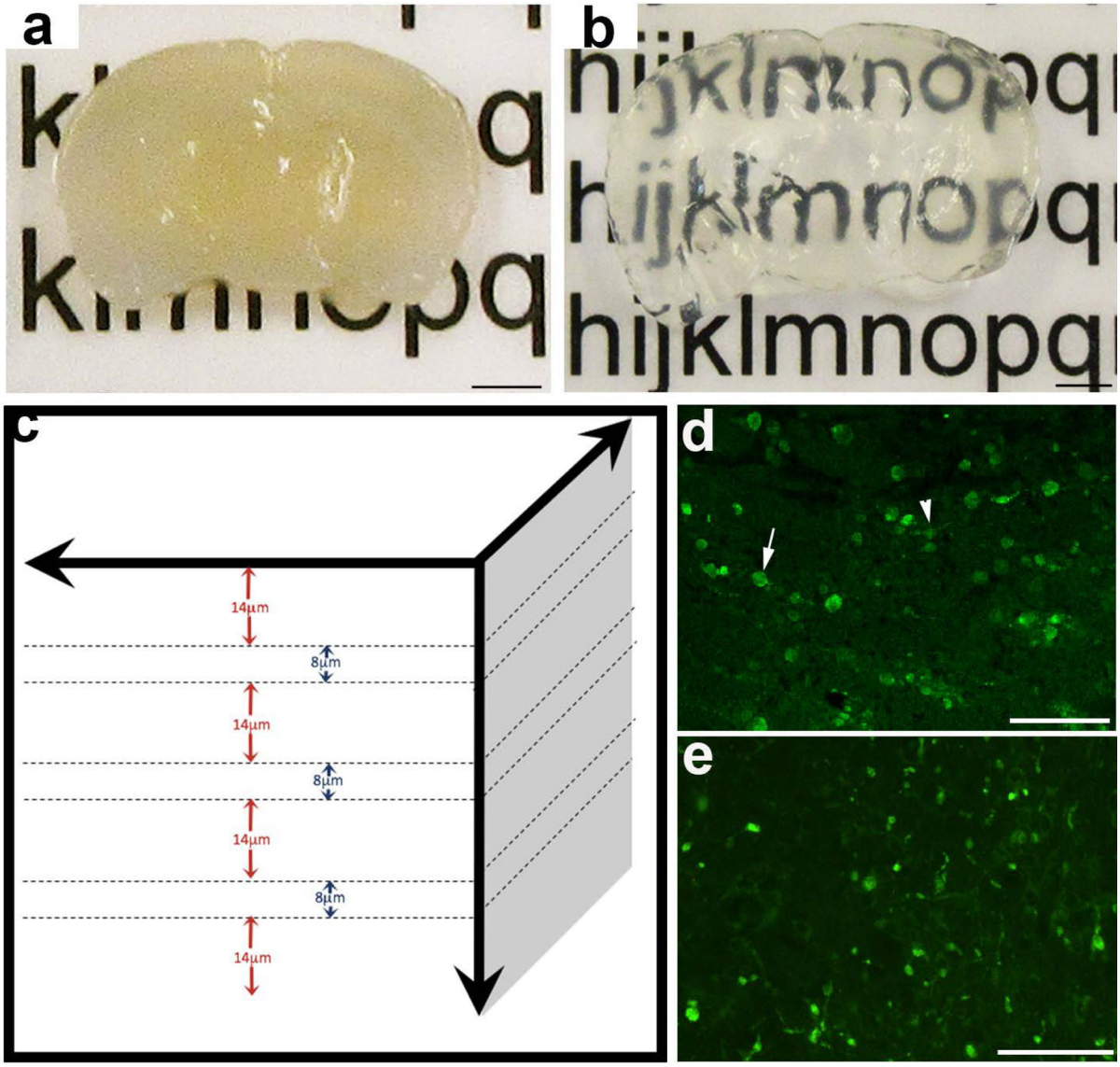

Figure 1. Evaluation of Axonal Pathology using the CLARITY Technique

Representative example of 2mm-thick block of uninjured mouse brain sectioned in the coronal plane **(a)** before and **(b)** after tissue clearing. **(c)** Diagram demonstrating the approach to analysis of cleared tissue. Specifically, 8μm regions of tissue were flattened (maximum-projection function) to simulate traditional formalin-fixed paraffin-embedded (FFPE) tissue sections. Bulbs identified within these regions were re-evaluated with the full 3D of tissue up to 100μm to determine their true morphology and connectivity status. 14μm gaps were included to avoid measurement of the same bulbs twice (based on maximal bulb size). **(d)** Representative example of standard 8μm-thick FFPE mouse tissue section immunofluorescently labelled with APP. Axonal swellings can be observed in the peri-contusional region at 24 hours following CCI. Note, while the vast majority of APP swellings appear as disconnected, terminal axonal bulbs (arrow), occasional varicosities can be observed with two clear projections from a single swelling along an intact axon

(arrowhead). **(e)** APP immunoreactive axonal pathology observed peri-contusionally at 24 hours post-CCI on 8μm-thick maximum projection images using cleared tissue appears indistinguishable from standard FFPE immunofluorescent sections in **(d)**. Scale bars: **(a,b)** 2mm, **(d,e)** 50μm.

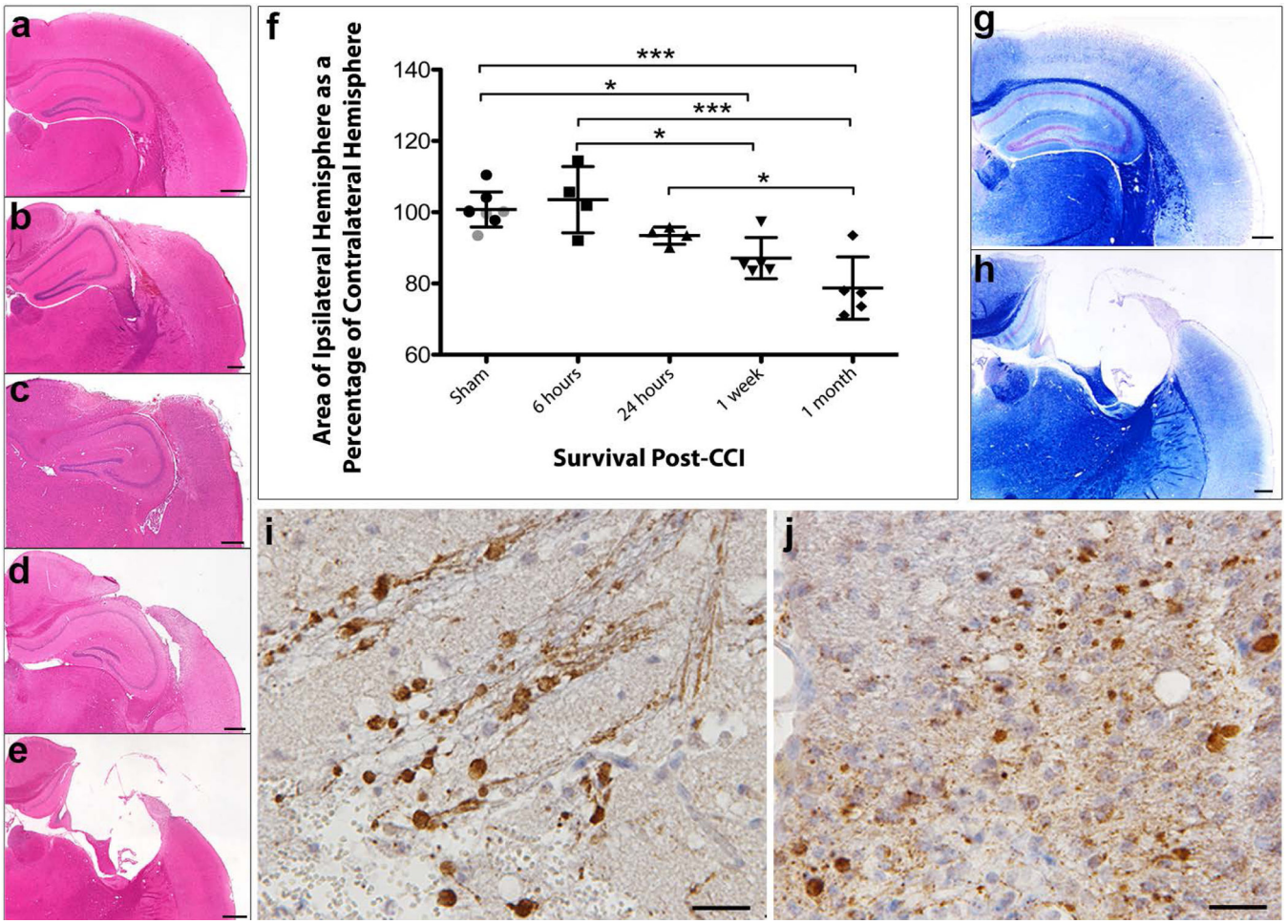

Figure 2. Progressive Atrophy and Associated Axonal Pathology Post-CCI in Standard FFPE Tissue

(a) H&E staining on sham animals reveals an absence of any focal pathology and a morphologically normal cortical surface. **(b-e)** H&E staining performed **(b)** 6 hours, **(c)** 24 hours, **(d)** 1 week and **(e)** 1 month after CCI injury reveals acute cortical contusion and intraparenchymal hemorrhage at the site of impact as well as progressive atrophy of the ipsilateral hemisphere. **(f)** Tissue atrophy quantified by measuring the area of the injured ipsilateral hemisphere as a percentage of the contralateral hemisphere. All individual data are presented in addition to the mean percentage area ± SD. In the sham group, gray data points indicate mice sacrificed 24 hours after sham injury and black data points indicate mice sacrificed 1 month following sham injury, indicating an absence of change caused by craniectomy. **(g–h)** Luxol fast blue staining indicates loss of white matter and major cortical tissue loss at **(h)** 1 month following injury compared to **(g)** sham. **(i–j)** Swollen axonal profiles and varicosities immunroeactive for APP at **(i)** 24 hours and **(j)** 1 month post-CCI. Scale bars: **(a–e, g–h)** 400μm, **(i–j)** 25μm. *p<0.05, ***p<0.0001

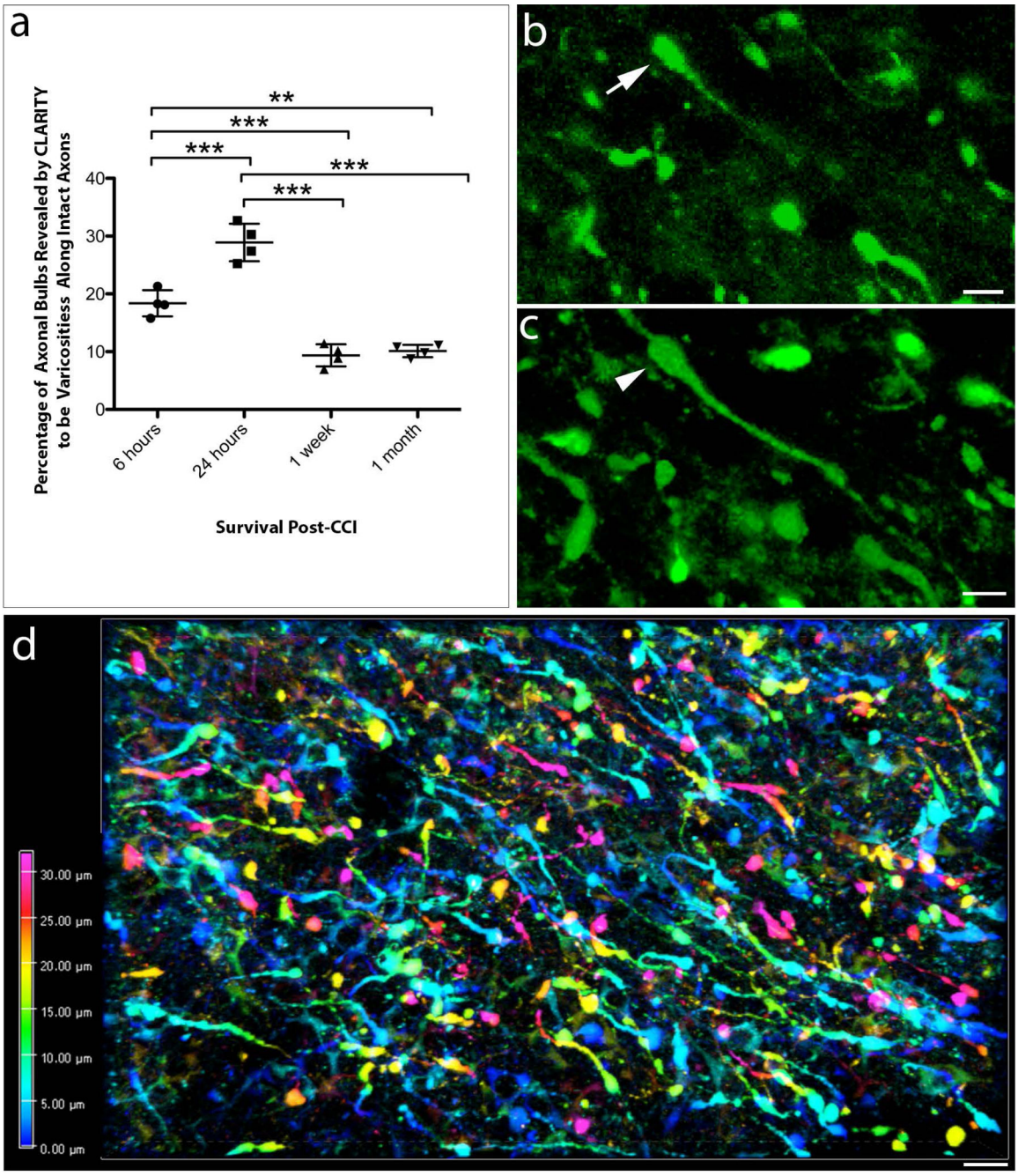

Figure 3. CLARITY Reveals Less Axonal Disconnection than Previously Thought Following CCI

(a) Graph showing the percentage of APP+ swellings that appeared terminally disconnected when viewed in standard 8μm-thick regions of tissue that were revealed to be connected varicose axonal swellings when all three-dimensions were fully visible using CLARITY (**p ≤ 0.01, ***p≤ 0.001). **(b)** Representative example of an APP+ apparent terminal axonal bulb (arrow) observed on an 8μm-thick region of cleared tissue (maximum projection) at 24 hours post-CCI. **(c)** The same region of tissue as (b) re-evaluated with all three-dimensions now visible reveals that the apparent bulb is in fact a swelling that has two clear projections and thus represents a varicose swelling along an intact region of axon (arrowhead). (Alpha-

blended image) **(d)** Depth encoded three-dimensional region of extensive APP+ axonal pathology in the peri-contusional region 24 hours post-CCI. Extensive and large axonal swellings can be observed with complex morphologies comprising both disconnected axonal bulbs and varicosities along the intact length of axons. Scale bars: **(b, c)** 10μm, **(d)** 50μm.

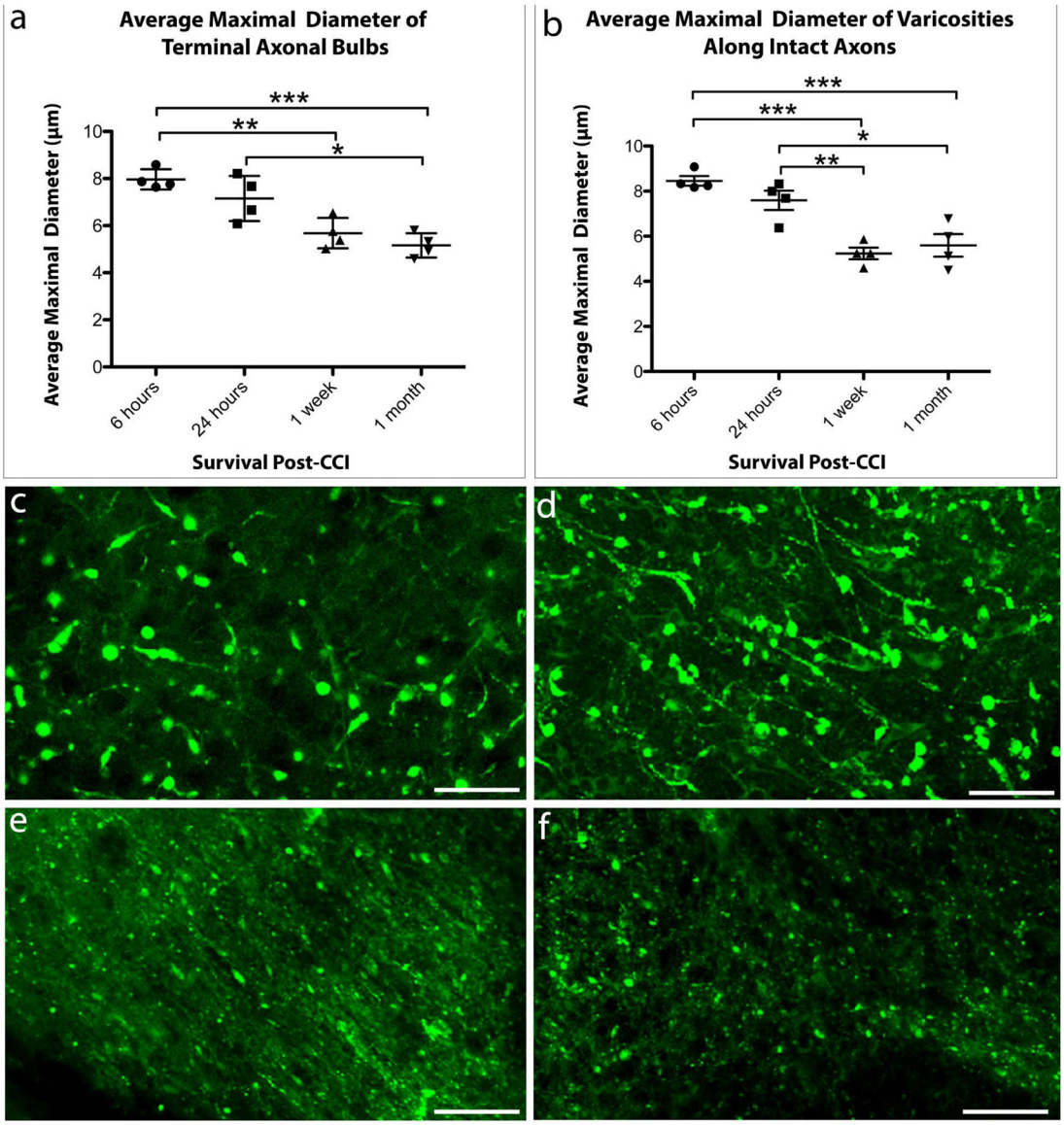

Figure 4. The Size of Axonal Swellings Decreases with Increased Survival Post-CCI

The average maximal diameter of axonal swellings of both **(a)** terminally disconnected bulbs and **(b)** axonal varicosities along intact axons decreases over time following CCI. (*p ≤ 0.05, **p ≤ 0.01, ***p ≤ 0.001, **** p ≤ 0.0001). **(c–f)** Representative examples of the relative size of axonal swellings in the peri-contusional region in cleared tissue at **(c)** 6 hours, **(d)** 24 hours, **(e)** 1 week, and **(f)** 1 month post-CCI. Scale bars: **(c–f)** 20µm.

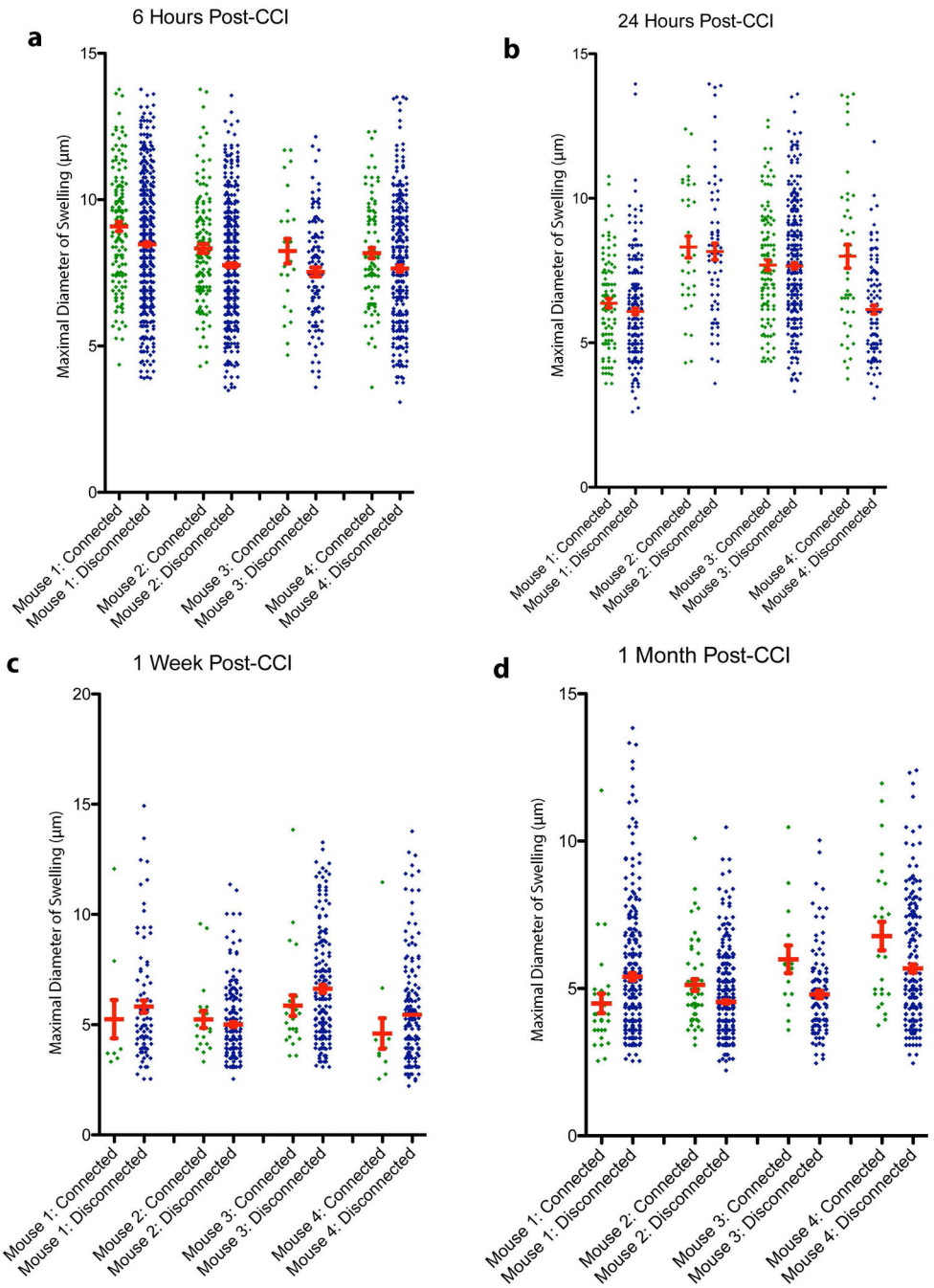

Figure 5. The Size of Axonal Swellings Changes Versus Connection Status with Survival.

The maximal diameter for all individual disconnected, terminal axonal bulbs and connected axonal varicosities shown for each mouse at **(a)** 6 hours, **(b)** 24 hours, **(c)** 1 week, and **(d)** 1 month post-CCI.